Structural characterization of CHCHD5 and CHCHD7: Two atypical human twin CX$_9$C proteins

Lucia Banci [a,b,*], Ivano Bertini [a,*], Simone Ciofi-Baffoni [a,b], Deepa Jaiswal [a], Sara Neri [a,b], Riccardo Peruzzini [a,b], Julia Winkelmann [a]

[a] Magnetic Resonance Center CERM, University of Florence, Via Luigi Sacconi 6, 50019 Sesto Fiorentino, Florence, Italy
[b] Department of Chemistry, University of Florence, Via della Lastruccia 3, 50019 Sesto Fiorentino, Florence, Italy

ARTICLE INFO

ABSTRACT

Twin CX$_9$C proteins constitute a large protein family among all eukaryotes; are putative substrates of the mitochondrial Mia40-dependent import machinery; contain a coiled coil-helix-coiled coil-helix (CHCH) fold stabilized by two disulfide bonds as exemplified by three structures available for this family. However, they considerably differ at the primary sequence level and this prevents an accurate prediction of their structural models. With the aim of expanding structural information on CHCH proteins, here we structurally characterized human CHCHD5 and CHCHD7. While CHCHD5 has two weakly interacting CHCH domains which sample a range of limited conformations as a consequence of hydrophobic interactions, CHCHD7 has a third helix hydrophobically interacting with an extension of helix α2, which is part of the CHCH domain. Upon reduction of the disulfide bonds both proteins become unstructured exposing hydrophobic patches, with the result of protein aggregation/precipitation. These results suggest a model where the molecular interactions guiding the protein recognition between Mia40 and the disulfide-reduced CHCHD5 and CHCHD7 substrates occurs *in vivo* when the latter proteins are partially embedded in the protein import pore of the outer membrane of mitochondria.

© 2012 Elsevier Inc. All rights reserved.

1. Introduction

Almost all of the proteins of the mitochondrial intermembrane space (IMS) are encoded by nuclear genes. These proteins are synthesized in the cytosol and then imported into mitochondria. While essentially all proteins directed to the matrix possess a targeting sequence which, by interacting with the translocases located in the outer and inner mitochondrial membranes, directs them to the matrix, different mechanisms can be operative for the import of nuclear encoded proteins into the IMS (Neupert and Herrmann, 2007). Many IMS proteins lack the mitochondrial targeting sequence and are characterized by conserved twin CX$_n$C (typically n = 3 and 9) motifs, which were found to mediate their import into the IMS through a disulfide relay system (Mesecke et al., 2005). Two proteins, Mia40 and ALR (named Erv1 in yeast), are the central components of this system (Hell, 2008). In particular, Mia40 is an oxidoreductase which promotes an oxidative folding process of the imported substrates through a thiol-disulfide exchange mechanism, in this way trapping them in the IMS (Chacinska et al.,

2004;Banci et al., 2009, 2010;Terziyska et al., 2009), while ALR/Erv1 restores the functional oxidized state of Mia40 (Terziyska et al., 2007;Lionaki et al., 2010;Banci et al., 2012).

Twin CX$_9$C proteins constitute a large protein family among all eukaryotes (Cavallaro, 2010). Yeast *Saccharomyces cerevisiae* contains 17 members, most of them required for the assembly or stability of respiratory chain complexes (Longen et al., 2009). In the human genome 29 genes were identified, eleven of them being part of respiratory chain complexes, twelve involved in cytochrome *c* oxidase assembly function and in the maintenance of fundamental structural and functional properties of mitochondria, and six with unknown function (Cavallaro, 2010). All twin CX$_9$C proteins contain a coiled coil-helix-coiled coil-helix (CHCH) domain as exemplified by the structures of Cox17 (PDB-ID: 2RN9) (Banci et al., 2008b;Abajian et al., 2004;Arnesano et al., 2005), Mia40 (PDB-ID: 2K3J) (Banci et al., 2009;Kawano et al., 2009) and p8-MTCP1 (PDB-ID: 1HP8) (Barthe et al., 1997). In all of them, the twin CX$_9$C motif forms two structural disulfides in a α-hairpin conformation blocking the two helices in an antiparallel orientation. Cox17 is the mitochondrial copper chaperone which is involved in copper transfer to cytochrome *c* oxidase (Horng et al., 2004;Banci et al., 2007b, 2008a). It binds a copper(I) ion through an additional CC motif in the N-terminal region (Banci et al., 2008b). Recently, the structure and functional role of Mia40 has

been extensively characterized, showing that its CPC motif in the N-terminal region is responsible for the introduction of disulfide bonds in the protein substrates (Banci et al., 2009;Grumbt et al., 2007). Mia40 functions as a molecular chaperone assisting the α-helical folding of an internal targeting signal (ITS) of the substrate (Banci et al., 2010;Sideris et al., 2009). p8-MTCP1 is a mitochondrial protein thought to be involved in T-cell proliferation and has been reported to play a potential role in leukemogenesis but its function is so far unknown (Madani et al., 1995;Soulier et al., 1994).

Although all CX$_9$C proteins presumably preserve a disulfide-bonded α-hairpin conformation, they have a large range of sequence lengths and a very low degree of sequence similarity both within a specific organism and in the orthologs of different species (Cavallaro, 2010;Longen et al., 2009). Therefore, these features do not allow to easily predict accurate structural models for this protein family. With the aim of expanding the structural information on CHCH proteins, we have structurally characterized two members of them, CHCHD5 and CHCHD7, in their fully oxidized states. The former protein has the peculiarity of containing two CHCH domains and is homologous to yeast Mic14 whose depletion affects mitochondrial oxygen consumption without influencing the mitochondrial cytochrome *c* oxidase and reductase activities (Longen et al., 2009). The latter protein is the homologue of yeast Cox23 which is required for cytochrome *c* oxidase assembly (Longen et al., 2009;Cavallaro, 2010;Barros et al., 2004). However, CHCHD7 has a very different sequence length compared to Cox23 (human 85 aa vs. yeast 151 aa).

2. Materials and methods

2.1. Bioinformatic analysis

Sequences homologous to those of the CHCHD5 and CHCHD7 proteins were searched via BLAST (http://blast.ncbi.nlm.nih.gov/Blast.cgi) in the database of non-redundant protein sequences using Blastp (protein–protein BLAST). Sequence alignments were performed using the ClustalW program with default parameters (Larkin et al., 2007). Prediction of the mitochondrial N-terminal targeting sequence has been performed through MitoProt II (Claros, 1995). The CHCHD7 and CHCHD5 sequences were submitted to the I-TASSER online modeling program. The I-TASSER server generates 3D atomic models by conducting multiple folding simulations on the basis of templates that it identifies as structural homologs in the Protein Data Bank (Roy et al., 2010;Zhang, 2008). The C-score, which is a confidence score for estimating the quality of predicted models by I-TASSER, is typically in the range of [−5,2], where a C-score of higher value signifies a model with a high confidence (Zhang and Skolnick, 2004). Our best models of CHCHD7 and CHCHD5 have a C-score of −1.58 and −1.75, respectively. For both proteins the TM-score, which is another parameter that measures the quality of the modeling prediction (Zhang and Skolnick, 2004), is 0.50 ± 0.15. A TM-score >0.5 indicates a model of correct topology. Both C- and TM-scores indicate that no reliable structural models were obtained. Moreover, the cysteines of the four CX$_9$C motifs in the I-TASSER model of CHCHD5 are not involved in the disulfide bonds typical of this protein family, thus indicating its unreliability.

2.2. Molecular cloning, expression and purification of CHCHD7 and CHCHD5

The cDNA (GenScript) coding for the human CHCHD7 or CHCHD5 proteins were cloned into pET16b and pET15 (Novagen),

respectively, using the restriction enzymes 5′ NdeI and 3′ BamHI (Fermentas), generating N-terminal His-tagged proteins.

The expression vector encoding for the full-length proteins (CHCHD7 and CHCHD5) was transformed into competent *Escherichia coli* BL21-Origami(DE3) cells (Stratagene), which were grown at 37 °C in Luria–Bertani, or in minimal medium ((^{15}NH$_4$)$_2$SO$_4$ and/or [^{13}C]glucose) for the production of labeled samples. Protein expression was induced at OD 0.7–0.8 with 0.5 mM isopropyl β-ᴅ-thiogalactopyranoside for 16 h at 25 °C. Cells were harvested by centrifugation at 11000*g* for 20 min and resuspended in lysis buffer (50 mM phosphate buffer pH 7.4, 0.5 M NaCl, 10 mM imidazole). Cell lysis was performed by sonicating with eight bursts of 30 s each. The suspension was centrifuged for 40 min and the supernatant was applied on a 5-ml Ni (or Zn)-charged Hi-Trap chelating HP column (Amersham Pharmacia Biotech). Unbound proteins were washed with binding buffer (50 mM phosphate buffer pH 7.4, 0.5 M NaCl, 100 mM imidazole) and CHCHD7$_{2S–S}$ or CHCHD5$_{4S–S}$ was eluted with elution buffer (50 mM phosphate buffer 7.5, 0.5 M NaCl, 500 mM imidazole). The CHCHD5 protein was then concentrated by ultrafiltration and loaded on a 16/60 Superdex 75 chromatographic column (Amersham Biosciences) to separate the dimeric (30%) from the monomeric protein-containing fractions (in 100 mM Tris, 100 mM NaCl, pH 8.0). This dimeric form of CHCHD5 protein results from the formation of unspecific intermolecular disulfide bond(s) as analyzed by SDS–PAGE with and without dithiothreitol (DTT). CHCHD7$_{2S–S}$ and monomeric CHCHD5$_{4S–S}$ were then concentrated by ultrafiltration and the His-tag was cleaved by incubation with factor Xa (50 mM Tris–HCl, 100 mM NaCl, 5 mM CaCl$_2$, pH 8) or Thrombin (100 mM Tris–HCl, 100 mM NaCl, pH 8.0) over night at room temperature or 4 °C, respectively. A second HiTrap chelating HP column was used to isolate the untagged CHCHD7$_{2S–S}$ or CHCHD5$_{4S–S}$, which were then loaded on a 16/60 Superdex 75 chromatographic column (50 mM KPi, pH 7.0) and concentrated by ultrafiltration to produce the final NMR sample. Yields of pure proteins were between 5–10 mg per liter of culture.

A N-ter CHCHD5 construct (a.a. 1–49) was obtained through the insertion of a stop codon (TAA) after Pro49 in the full-length construct. QuikChange XL Site-Directed Mutagenesis Kit from Stratagene was used for the mutagenesis reaction with the following forward primer, GTACGAGCTCTCACCCGTAAATTATTCGCCAGATT CGC. N-ter CHCHD5$_{2S–S}$ protein (a.a. 1–49) was expressed and purified following the same protocol of the full-length protein, with the exception that the first gel filtration was omitted as the protein eluted from the HiTrap chelating column in the monomeric form only.

A C-ter CHCHD5 construct (a.a. 50–110) was obtained through the insertion of NdeI restriction enzyme recognition site (CATATG) after Pro49 by site-directed mutagenesis, using the following forward primer, GTACGAGCTCTCACCCGTAACATATGATTATTCGCCA-GATTCGCC. The C-ter CHCHD5 construct was sub-cloned using NdeI and BamHI restriction enzymes in pET15 expression vector. Protein expression and purification were performed following the same protocol of the N-ter construct.

2.3. Mass Spectrometry

MALDI-MS experiments were performed on Bruker DaltonicsUltraflex III MALDI TOF/TOF instrument in order to confirm the molecular mass of the purified protein. 1 μl of protein solution was mixed with 1 μl of matrix solution (SA 10 mg/ml in 70% acetonitrile/30% water, 0.1% TFA) and analyzed. Flex Control 3.0 was used as data acquisition software in positive linear mode. The instrument was externally calibrated prior to analysis using the Bruker Protein calibration standard kit.

2.4. Analytical gel filtration chromatography

The aggregation state of CHCHD7$_{2S-S}$ and of the various constructs of CHCHD5$_{4S-S}$ (full length, N-ter and C-ter constructs) was analyzed using analytical gel filtration approach. Purified samples were run on ÄKTAFPLC™ using a Superdex 200 HR 10/300 analytical column or a Superdex 75 HR 10/300 analytical column (GE Healthcare). Fifty millimolar sodium phosphate, 150 mM NaCl buffer pH 7.0 was used as eluent with a flow rate of 0.6 ml/min. Standard proteins used for the calibration curve were aprotinin, ribonuclease A and ovalbumin.

2.5. Reduction of CHCHD7$_{2S-S}$ and CHCHD5$_{4S-S}$

For the reduction of protein disulfide bonds, degassed 50 mM phosphate buffer pH 7.0 was used and up to 300 mM DTT or 25 mM tris(2-carboxyethyl)phosphine was added. The effect of cysteine reduction on the folding properties was analyzed through NMR ^{1}H–^{15}N HSQC experiments at 800 MHz. The reducing agent was then removed from the reduced protein using a PD10 column or by dialysis, and the cysteine redox state investigated through protein alkylation followed by SDS–PAGE. The proteins were reacted with 4-acetamido-4′-maleimidylstilbene-2,2′-disulfonate (AMS) which specifically alkylates reduced cysteines increasing the molecular weight by 500 Da per cysteine residue.

2.6. Circular dichroism

Far-UV CD analyses of CHCHD5 (20 μM) and CHCHD7 (13 μM) were performed in 50 mM phosphate buffer pH 7.0 with the addition of different amounts of DTT. Spectra were acquired at 298 K using a 1-mm path-length cell and a Jasco J-810 spectropolarimeter (Jasco, Tokyo, Japan). All spectra were recorded with an average of 5 accumulations at a scan speed of 20 nm/min and at a response time of 2 s. The relative α-helical content was calculated from the mean residue ellipticity value at 222 nm for the indicated DTT concentration taking the value at 0 mM DTT as 100%.

2.7. NMR relaxation experiments and analysis

^{15}N R_1, R_2, and steady-state heteronuclear NOE measurements were performed at 500 or 600 MHz, 298 and/or 308 K, using the pulse sequences previously reported (Farrow et al., 1994;Grzesiek and Bax, 1993) on ^{15}N-labeled samples. The overall rotational correlation time values were estimated from the R_2/R_1 ratio using the program QUADRATIC_DIFFUSION (Lee et al., 1997). The relaxation data for those NHs having an exchange contribution to the R_2 value or exhibiting large-amplitude fast internal motions, as monitored by low NOE values, were excluded from the analysis (Kay et al., 1989;Tjandra et al., 1995).

Estimates of the molecular tumbling value under the chosen experimental conditions of magnetic field and temperature were
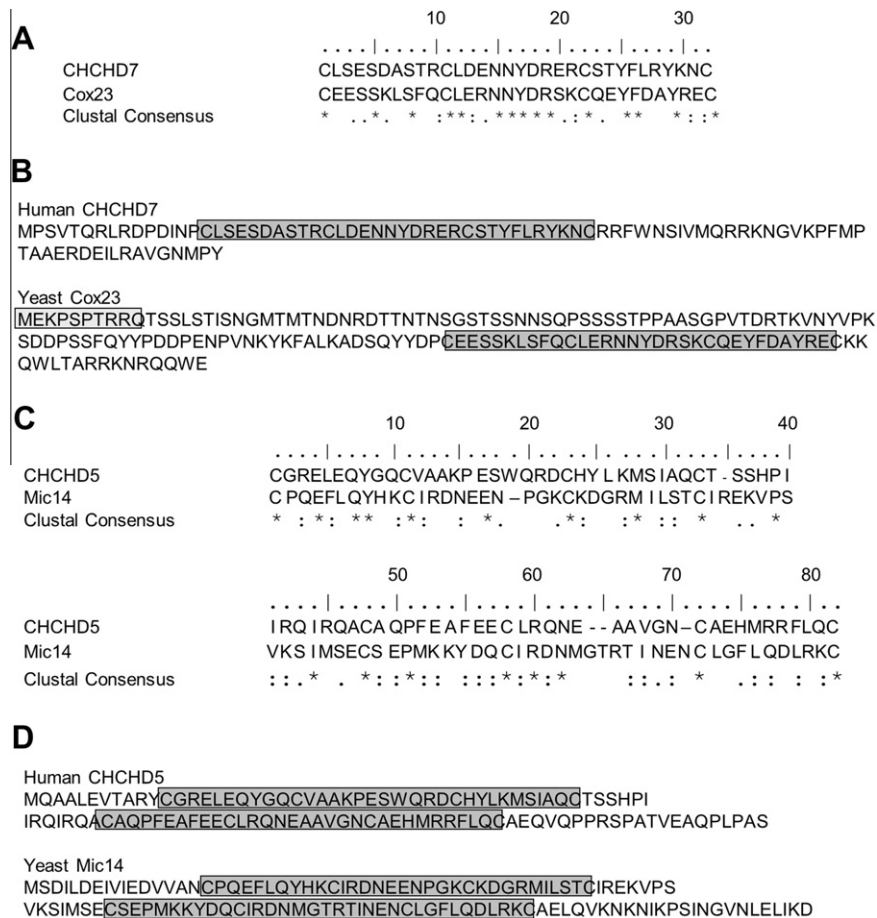

Fig.1. Sequence comparison between the human CHCHD7 or CHCHD5 and their yeast homologues. Alignment between the CHCH domains of the human CHCHD7 (A) and CHCHD5 (C) and their yeast homologues (Cox23 and Mic14, respectively) starting with the first Cys and ending with the fourth Cys of each CHCH domain. Identical residues are marked by an asterisk. Location of the CHCH domains (shaded in grey) in the amino acid sequences of CHCHD7 (B)/CHCHD5 (D) and Cox23 (B)/Mic14 (D) and the putative mitochondrial targeting peptide at the N-terminus of Cox23 (shaded in light grey).

obtained using the program HydroNMR following the standard procedure (Garcia de la Torre et al., 2000). The input structures do not contain the first 15 residues (CHCHD7$_{2S-S}$), and the first 10 and the last 15 residues (CHCHD5$_{4S-S}$) as they are unstructured.

The experimental longitudinal and transverse relaxation rates and the heteronuclear NOEs of CHCHD7$_{2S-S}$ recorded at 500 MHz and 298 K have been analyzed with the TENSOR 2.0 program (Dosset et al., 2000), which allows the determination of rotational diffusion from three-dimensional structure coordinates and experimental ^{15}N relaxation data and to perform a model-free analysis of local internal mobility affecting backbone amides in the presence of an isotropic or anisotropic rotational diffusion tensor (Tsan et al., 2000;Dosset et al., 2000).

2.8. NMR experiments and structure calculations

All NMR spectra to obtain the solution structures of CHCHD7$_{2S-S}$ and CHCHD5$_{4S-S}$ were recorded at 298 and 308 K, respectively, using Bruker Avance 500, 700 and 900 MHz spectrometers, processed using the standard Bruker Topspin software and analyzed by CARA program (Keller, 2004). The NMR experiments used for resonance assignment and structure calculations were performed on ^{13}C-/^{15}N-labeled or on ^{15}N-labeled samples (0.5–1 mM) in 50 mM phosphate buffer pH 7 containing 10% (v/v) D$_2$O. The ^{1}H,

^{13}C, and ^{15}N backbone resonance assignment of CHCHD7$_{2S-S}$ and of the various constructs of CHCHD5 was performed using standard triple-resonance NMR experiments. The side chain assignment of CHCHD7$_{2S-S}$ and CHCHD5$_{4S-S}$ was performed using TOCSY- and NOESY-based NMR experiments. Secondary structure analysis has been performed by PECAN (Eghbalnia et al., 2005), CSI (Wishart et al., 1992) and TALOS+ (Shen et al., 2009).

^{1}H–^{15}N HSQC spectra of CHCHD5$_{4S-S}$, recorded in the presence and in the absence of TEMPOL (4-hydroxy-2,2,6,6-tetramethyl-piperidine-1 oxyl, 97% purity, Sigma–Aldrich) from a Bruker Avance700 spectrometer with 512 increments and 32 scans over 1024 data points, were compared to determine paramagnetic perturbations on signal intensities. Paramagnetic sample (0.7 mM) contained an optimal 20 mM TEMPOL concentration, which was achieved by adding directly to the NMR tube a few microliters of a 2 M TEMPOL stock solution in 99.9% D$_2$O. Only well resolved NMR signals were selected and their volumes analyzed according to the standard procedure (Molinari et al., 1997).

Structure calculations were performed with the software package UNIO (ATNOS/CANDID/CYANA) (Herrmann et al., 2002a,b;Güntert, 2004), using as input the amino acid sequence, the chemical shift lists, three [^{1}H,^{1}H]-NOE experiments (two-dimensional NOESY, three-dimensional ^{15}N-resolved NOESY and three-dimensional ^{13}C-resolved NOESY), and backbone torsion
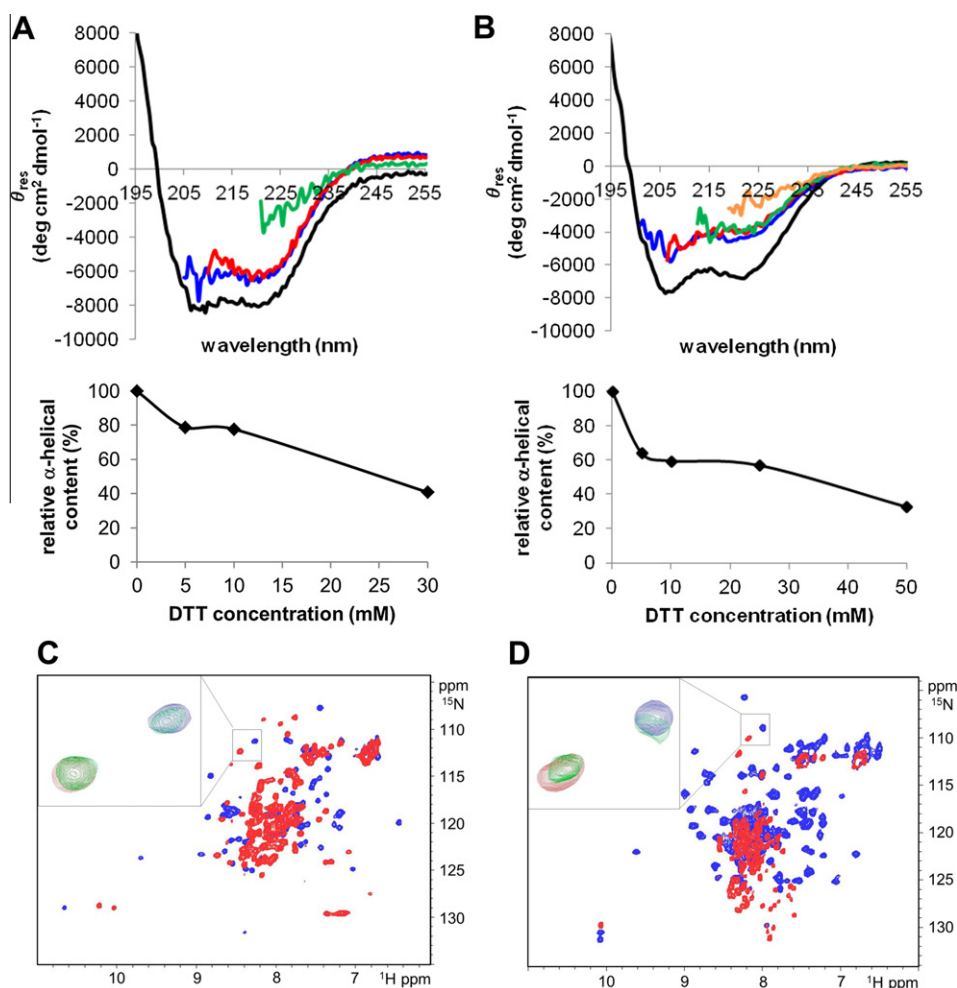

Fig.2. Redox state-dependent structural properties of CHCHD7 and CHCHD5. The mean residue molar ellipticity (θ_{res}) of CHCHD7$_{2S-S}$ (A) and CHCHD5$_{4S-S}$ (B) in the absence (black line) and in the presence of different DTT concentrations (5 (blue), 10 (red), 30 or 25 (green), 50 mM (orange)). The relative α-helical content as a function of DTT concentration is reported for both proteins. ^{1}H–^{15}N HSQC maps of CHCHD7$_{2S-S}$ (C) and CHCHD5$_{4S-S}$ (D) at 298 K and 800 MHz and 500 MHz, respectively, in the absence of DTT (blue) and in the presence of 200 mM DTT (red). An overlay of ^{1}H–^{15}N HSQC maps at increasing DTT concentration is shown for a selected region for each protein. Starting point (0 mM DTT) is in blue, addition 1 (50 mM DTT final concentration) is in green, addition 2 (100 mM DTT final concentration) is in red.

angle constraints, derived from ^{1}H, ^{13}C and ^{15}N chemical shift analysis performed with TALOS+ program (Shen et al., 2009). The 20 conformers with the lowest residual target function values were subjected to restrained energy minimization in explicit water with the program AMBER 10 (Case et al., 2008). The quality of the structures was evaluated by the programs PSVS (Bhattacharya et al., 2007) and iCing (http://nmr.cmbi.ru.nl/cing/iCing.html). The conformational and energetic analysis of the final restrained energy minimized family of 20 conformers of CHCHD5$_{4S-S}$ and CHCHD7$_{2S-S}$ are reported in Tables S1 and S2, respectively. The atomic coordinates, structural restraints and resonance assignments of CHCHD5$_{4S-S}$ and CHCHD7$_{2S-S}$ have been deposited in the Protein Data Bank and BioMagResBank (PDB-ID: 2lql, BMRB accession number: 18318 for CHCHD5; PDB-ID: 2lqt, BMRB accession number: 18328 for CHCHD7).

3. Results

3.1. Bioinformatic analysis of CHCHD5 and CHCHD7

Human CHCHD7 has been reported to be the homologous protein of yeast Cox23 (Longen et al., 2009;Cavallaro, 2010) which has been detected in the IMS (Barros et al., 2004). In both proteins the CHCH domain (starting with the first Cys and ending with the fourth Cys) comprises 32 amino acids. The identity between the two CHCH domains is 46% (Fig. 1A) but the sequence pattern of the two proteins shows significant differences. While the yeast protein is constituted by 151 amino acids and contains a putative N-terminal mitochondrial targeting sequence, the human protein is formed by only 85 amino acids with no predicted mitochondrial targeting sequence (Fig. 1B). Moreover, in the yeast protein the CHCH domain is located in the C-terminal region with additional 103 amino acids at the N-terminus while in the human protein it is found in the N-terminal region with a C-terminal extension of 38 residues (Fig. 1B). The yeast homologue of the human protein CHCHD5 is termed Mic14 (mitochondrial IMS cysteine motif protein of 14 kDa) (Longen et al., 2009;Cavallaro, 2010). In both organisms the protein has two CHCH domains separated by 13/14 amino acids, each of the domain containing four conserved cysteine residues, with a pairwise identity of 21% and no predictable N-terminal mitochondrial targeting sequence (Fig. 1C and D).

The mitochondrial IMS-targeting signal (ITS) is a sequence stretch found in essentially all CHCH, Mia40-dependent substrates. The ITS primes one Cys for docking with Mia40's CPC motif which is responsible for the introduction of a disulfide bond in the substrate (Sideris et al., 2009;Milenkovic et al., 2009). The ITS is defined as a stretch of at least nine amino acids upstream or downstream of any cysteine of the $CX_9CX_nCX_9C$ motif, and having two hydrophobic amino acids four and seven amino acids distant from the docking cysteine (Sideris et al., 2009;Milenkovic et al., 2009). Such putative ITS sequence stretches were predicted for both CHCHD7 and Cox23 downstream of the third or fourth cysteine residue and, for Cox23, additionally upstream of the fourth cysteine, suggesting that they are potential Mia40 substrates. Mic14 has been reported to be transported to the IMS by Mia40/Erv1 disulfide relay system (Gabriel et al., 2007) and putative ITS sequence stretches were predicted downstream of the first
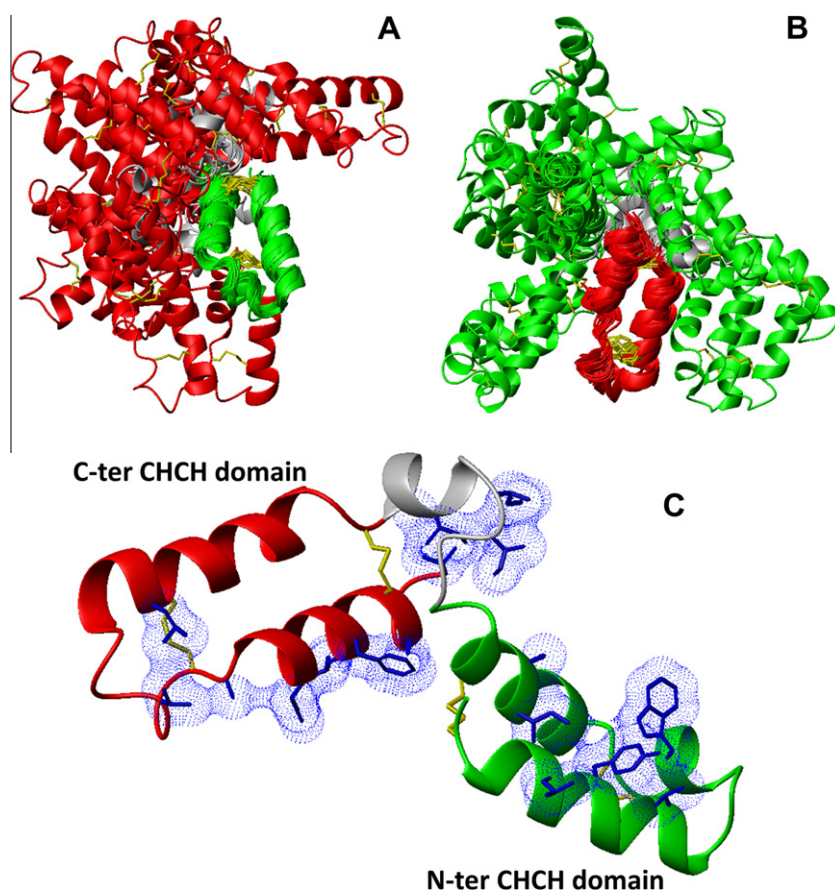

Fig.3. Solution structure of CHCHD5$_{4S-S}$. The bundle of 20 conformers representing the final NMR structure of CHCHD5$_{4S-S}$ is shown by superimposing the backbone atoms of the N-ter (A) and the C-ter (B) CHCH domain. (C) Ribbon presentation of one conformer of CHCHD5$_{4S-S}$ with residues involved in hydrophobic contacts colored in blue and with van der Waals contact surfaces. The N-ter CHCH domain is in green, the C-ter CHCH domain is in red, and the linker between the two domains is in grey. Disulfide bonds are in yellow. (For interpretation of the references to color in this figure legend, the reader is referred to the web version of this article.)

cysteine residue in both CHCH domains of Mic14. CHCHD5 has the same ITS regions and, additionally, another one downstream of the third cysteine in the second CHCH domain, suggesting to be a Mia40 substrate, as Mic14. The ITSs present in these four proteins matched with those most commonly identified in the CHCH family, i.e. downstream of the first or of the third cysteine of the CHCH domain (Cavallaro, 2010).

Structural models of CHCHD7 and CHCHD5 generated through the I-TASSER server were not enough accurate to be considered representative of a correct structure (see Section 2.1 for details) and therefore we proceeded to solve the structure of both proteins experimentally through solution NMR.

3.2. Redox state-dependent properties of CHCHD5 and CHCHD7

MALDI-MS analysis revealed that recombinantly expressed and purified CHCHD7 and CHCHD5 have molecular weights of 10.2 and 12.7 kDa, respectively, in agreement with their theoretical values. SDS–PAGE analysis of the purified protein samples mixed with the thiol-reactive reagent 4-acetamido-4′-maleimidylstilbene-2,2′-disulfonic acid (AMS) (see Section 2.5 for details) showed a clear shift of the CHCHD7 and CHCHD5 bands only upon addition of a large excess of dithiothreitol (DTT) (data not shown). This indicates that the cysteine residues of purified CHCHD7 and CHCHD5 are involved in two ($CHCHD7_{2S-S}$ hereafter) and four ($CHCHD5_{4S-S}$ hereafter) disulfide bonds, respectively, while the cysteine residues are reduced after addition of the reducing agent and hence they are able to react with AMS.

Analytical gel filtration shows that $CHCHD7_{2S-S}$ is in a monomeric state (Fig. S1). The molecular tumbling value of $CHCHD7_{2S-S}$ (τ_m = 10.8 ± 1.1 ns at 298 K), estimated through NMR measuring ^{15}N backbone relaxation rates, is in agreement with the HYDRONMR-derived (Garcia et al., 2000) value of the protein in a monomeric state (8.9 ns). Also $CHCHD5_{4S-S}$ elutes in the analytical gel filtration as a single species but with an apparent molecular weight (MW_{app}) of ~19 kDa which is slightly higher than the value expected for a monomeric state (Fig. S1). However, the molecular tumbling time value (11.0 ± 1.2 ns at 298 K and 10.1 ± 1.5 ns at 308 K) is in the same range of that derived from HYDRONMR for a monomeric protein state (9.3 ± 0.8 ns at 298 K and 8.9 ± 0.8 ns at 308 K obtained averaging τ_m values calculated using the ensemble of 20 NMR conformers, see later). Therefore, the divergence between the experimental MW value obtained from the analytical gel filtration and the theoretical MW values can be ascribed to a non-globular protein shape of CHCHD5.

Circular dicroism (CD) spectra of $CHCHD7_{2S-S}$ and $CHCHD5_{4S-S}$ indicate that both proteins have α-helical secondary structure with typical negative minima around 208 and 222 nm (Fig. 2A and B). After incubation with an excess of DTT, the α-helical content decreases by 60% and 70%, respectively (Fig. 2A and B). These data indicate a high propensity of the proteins to adopt a α-helical conformation when the disulfide bonds are present, while upon their reduction the proteins acquire a largely unstructured state. To investigate the effect of disulfide bond reduction on the tertiary structure of $CHCHD7_{2S-S}$ and $CHCHD5_{4S-S}$, NMR spectra were recorded at various DTT concentrations. With increasing concentration of DTT, a slow exchange process on the NMR time scale is observed corresponding to the formation of the reduced state whose NH signal dispersion is largely decreased (Fig. 2C and D). The majority of backbone NHs in the final $^{1}H–^{15}N$ HSQC spectra
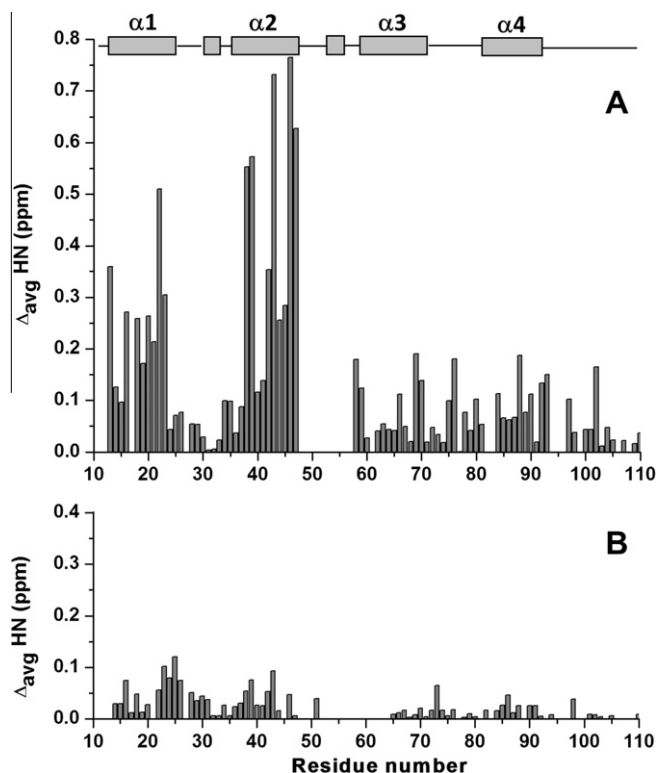

Fig.4. Interaction properties of the CHCH domains in $CHCHD5_{4S-S}$. The weighted-average chemical shift differences Δ_{avg} HN (that is, $([(\Delta H)^2 + (\Delta N/5)^2]/2)^{1/2}$, where ΔH and ΔN are chemical shift differences for ^1H and ^{15}N, respectively) between (A) the full-length protein and the N-ter and C-ter constructs and between (B) the ^{15}N-labeled N-ter construct before and after addition of the unlabeled C-ter construct and vice versa. Secondary structure elements of full-length $CHCHD5_{4S-S}$ are shown at the top.
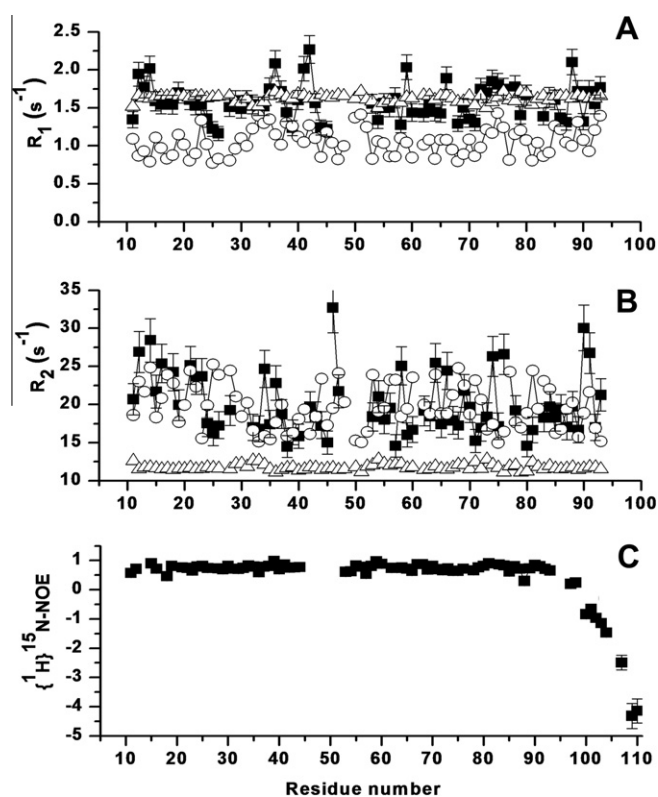

Fig.5. Experimental and calculated ^{15}N relaxation parameters of $CHCHD5_{4S-S}$. Experimental (filled squares) backbone ^{15}N R_1 (A) and R_2 (B) values for $CHCHD5_{4S-S}$ were compared with those values estimated from the atomic coordinates of the most compact (open triangle) and the most extended (open circle) conformer among the family of 20 conformers. (C) Experimental $^{15}N\{^1H\}$-NOE values for the full-length protein.

of both proteins are clustered in the spectral region typical of unfolded polypeptides (amide proton resonances clustered between 8 and 8.5 ppm). At variance with what has been observed for Cox17, namely that its fully reduced state is highly soluble (Banci et al., 2008b), protein aggregation and precipitation slowly occur in a day for both CHCHD5 and CHCHD7, thus preventing a detailed NMR characterization of their reduced states.

3.3. Structural characterization of CHCHD5$_{4S-S}$

The ^{1}H–^{15}N HSQC spectrum of CHCHD5$_{4S-S}$ protein shows well-spread resonances which indicate a folded protein. 88 out of 101 expected backbone amide resonances (excluding 8 proline residues and the first Met) were assigned. Backbone amide resonances were missing for residues at the N-terminus (2, 6–10), for some residues of the linker connecting the two CHCH domains (48–52) and for residues 17 and 82. Secondary structure analysis performed on the basis of ^{13}C$_\beta$, ^{13}C$_\alpha$, ^{13}CO, H$_\alpha$ chemical shifts showed the presence of the two expected twin α-helices forming the two CHCH domains. Accordingly, NMR ^{13}C$_{\alpha\beta}$ chemical shifts (Sharma and Rajarathnam, 2000) indicate that the eight cysteine residues of the two CHCH domains are involved in four disulfide bonds. The resonance assignment was also performed on two constructs which comprise the N-terminal (a.a. 1–49) and C-terminal (a.a. 50–110) CHCH domain, respectively (named N-ter and C-ter CHCHD5$_{2S-S}$ hereafter). The secondary structure analysis demonstrates the presence of the same α-helical stretches present in the CHCH domains of the full-length protein.

The solution structure of the full-length protein shows the presence of two α-helical hairpins which are well-ordered when individually superimposed (Fig. 3A and B, backbone RMSD$_{12-46}$ 0.86 Å and backbone RMSD$_{58-92}$ 1.27 Å), but sample several reciprocal conformations when considering the entire ensemble (backbone RMSD$_{12-92}$ 6.45 Å), consistently with the lack of interdomain NOEs and the missing assignment of 5 residues in the linker region (composed by 10 residues). The linker region is, however, not completely unstructured. Indeed, a α-helical segment, involving residues 52–57, is present in the ensemble of all 20 conformers (Fig. 3) as resulting from chemical shift index and TALOS+ analysis (Fig. S2). A short α-helix is also present in the loop connecting the disulfide-bridged α-helices in the first CHCH domain (Fig. 3C).

To investigate the interaction between the two CHCH domains, the ^{1}H-^{15}N HSQC map (Fig. S3) and the backbone chemical shifts of the full-length protein (Fig. 4A) were compared with those of the individual N-ter and C-ter CHCHD5$_{2S-S}$ constructs. Chemical shift variations are scattered across the two helices of the N-ter CHCH domain and involve few residues in the C-ter domain (Fig. 4A). No large chemical shift differences were however observed between the isolated domains when they are mixed in a 1:1 ratio (Fig. 4B). These data suggest that the two domains do not specifically recognize each other, consistent with the lack of interdomain NOEs in the full-length protein. However, the chemical shift variations measured for the residues in the N-ter CHCH domain indicate that the two CHCH domains are not fully independent.

To analyze the relative orientation of the CHCH domains, experimental ^{15}N R_1 and R_2 data of the full-length protein were compared with the values estimated from rigid-body hydrodynamic modeling using the atomic coordinates of the most compact and the most extended conformation of the two CHCH domains within the family of 20 conformers. As shown in Fig. 5A, the experimental R_1 values are, on average, matching the theoretical R_1 values of the most compact conformer. On the contrary, the experimental R_2 values are, on average, higher than those expected from the more compact conformation (Fig. 5B). This could be due to the presence of conformational exchange contributions occurring along the whole amino acid sequence. This behavior explains the low

number of NOE cross-peaks in the NH region of the 2D NOESY spectrum (Fig. S4, 539 cross-peaks at 298 K and 460 cross-peaks at 308 K), which is significantly less than would be expected for a protein of CHCH5's size and topology (550 cross-peaks at 298 K for human Cox17 which has only one CHCH domain). A similar behavior has been already reported in other systems (Bertini et al., 2003; Banci et al., 2007a), for which multiple conformational exchange processes occurring on a time-scale that is of the order of the reciprocal frequency separation determine dramatic exchange broadening which can easily render the NOE unobservable, especially when coalescence is approached. The experimental ^{15}N{^{1}H}-NOE values for CHCH5$_{4S-S}$ (Fig. 5C) demonstrate that the single domains forming the full-length protein behave as rigid bodies. Only sixteen residues at the C-terminus are very mobile as shown by its negative heteronuclear {^{1}H}^{15}N-NOEs, indicative of fast (nanosecond to picosecond) internal mobility. All together, ^{15}N NMR relaxation data indicate that the two CHCH domains in the full-length protein do not reorient independently in solution but they neither behave like a rigid body as they sample a range of limited conformations.

Paramagnetic profile of TEMPOL accessibility to the CHCH5$_{4S-S}$ surface was measured to provide further information on the relative orientation of the CHCH domains. TEMPOL is a soluble and stable free radical commonly employed for analyzing the distribution of protein surface hot spots (Bernini et al., 2009). Changes of ^{1}H–^{15}N signal intensities of backbone amides in HSQC protein spectra recorded in the presence and absence of 20 mM TEMPOL have been measured and reported as paramagnetic attenuations, Ai, following a well-known protocol (Molinari et al., 1997). A 20 mM TEMPOL concentration induces a sizeable broadening of NH signals but it
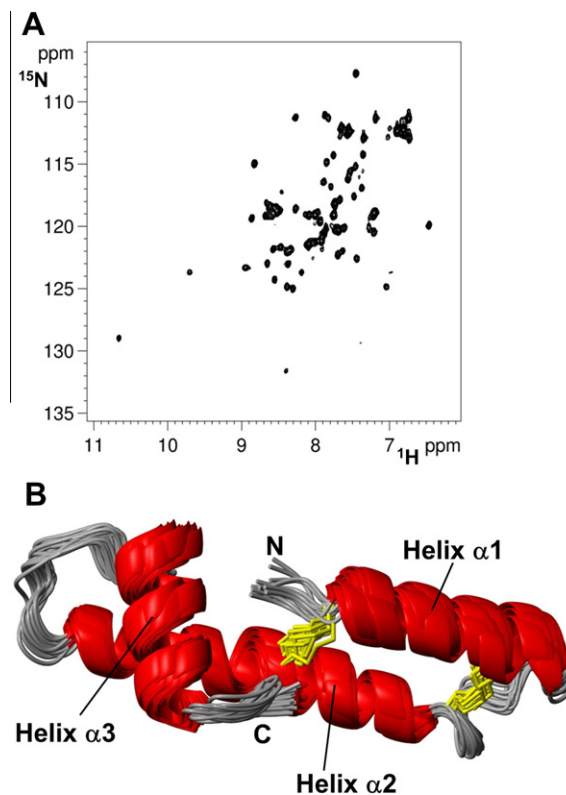

Fig.6. Structural properties of CHCHD7$_{2S-S}$. (A) ^{1}H–^{15}N HSQC spectrum of CHCHD7$_{2S-S}$ at 800 MHz and 298 K; (B) The bundle of 20 conformers representing the final NMR structure of CHCHD7$_{2S-S}$ is shown by superimposing the backbone atoms. Disulfide bonds are shown in yellow. (For interpretation of the references to color in this figure legend, the reader is referred to the web version of this article.)

does not generate too much loss in the signal/noise ratio. Chemical shifts are only marginally affected by the presence of 20 mM TEMPOL (mean absolute difference <0.02 ppm), a circumstance that makes assignments trivial. Ai values have been calculated for most of the CHCH5$_{4S-S}$ amide groups, i.e. 73 out of the total 88 assigned NH signals which are present in both diamagnetic and paramagnetic ^{1}H–^{15}N HSQC spectra. The obtained Ai values range from a maximum of 2.0 to a minimum of 0.6 for signals exhibiting strong and weak paramagnetic attenuations, respectively. The mean value of Ai is 1.12 and the residues whose NHs are attenuated by TEMPOL are spread all over the sequence of CHCH5$_{4S-S}$ (Fig. S5), indicating that both domains are accessible to the solvent. The TEMPOL induced Ai values were mapped to the surface of the most extended conformation of CHCH5$_{4S-S}$, and also plotted graphically (Fig. S5). All atoms of residues with the highest attenuations (2.0 < Ai < 1.4) are painted in red, those of residues with intermediate attenuations (1.4 < Ai < 1.2) are painted in orange. From this analysis it results that the residues whose NH correlations are most affected by TEMPOL are distributed all over the solvent exposed surface of the two CHCH domains in their relative most extended conformation. In agreement with the ^{15}N NMR relaxation data, this behavior indicates that the two domains are not strongly interacting with each other but they are largely solvent accessible in a not compact structural organization.

In conclusion, structural, chemical shift mapping, ^{15}N relaxation and paramagnetic relaxation enhancement data show that the CHCH5$_{4S-S}$ does not exhibit a rigid body hydrodynamics experiencing indeed a certain degree of motions between the two CHCH domains, which behave as rigid entities. The analysis of the hydrophobic contacts in the 20 conformers shows the presence of three main regions located (i) in the first α-hairpin domain, (ii) in the short α-helix of the linker region, (iii) in the second α-hairpin domain (Fig. 3C). The interactions of these hydrophobic regions could have a role in restricting the degree of flexibility of the two CHCH domains without locking them completely in one rigid conformation. These hydrophobic contacts can also be responsible for the aggregation and precipitation observed for the reduced state of the protein. Indeed, upon disulfide bond reduction, these hydrophobic residues can become completely solvent exposed, thereby enabling non-specific protein–protein interactions.

3.4. Structural characterization of CHCHD7$_{2S-S}$

The ^{1}H–^{15}N HSQC spectrum of CHCHD7$_{2S-S}$ shows well-spread resonances indicating a folded protein (Fig. 6A). 67 out of 78 expected backbone amide resonances (excluding 6 proline residues and the first Met) were assigned. Backbone amide resonances were missing for the N-terminal residues 3–10 as well as for residues 24, 39 and 45. Secondary structure analysis performed on the basis of ^{13}C$_{\beta}$, ^{13}C$_{\alpha}$, ^{13}CO, H$_{\alpha}$ chemical shifts showed that, in addition to the two α-helices of the CHCH-domain, a further α-helix is present in the C-terminal region of the protein. NMR ^{13}C$_{\alpha\beta}$ chemical shifts (Sharma and Rajarathnam, 2000) indicate that the four cysteine residues of the CHCH domain are involved in two disulfide bonds.

The solution structure shows that the three α-helices form a prolate, ellipsoidal-shaped molecule in which helix α3 is perpendicular to the polar axis (Fig. 6B). The N-terminal α-helix is formed by thirteen residues (17–29) as usually found in the CHCH fold, while the second α-helix, comprising residues 38–59, is unusually long compared to other CX$_9$C members (22 vs. 12 residues of
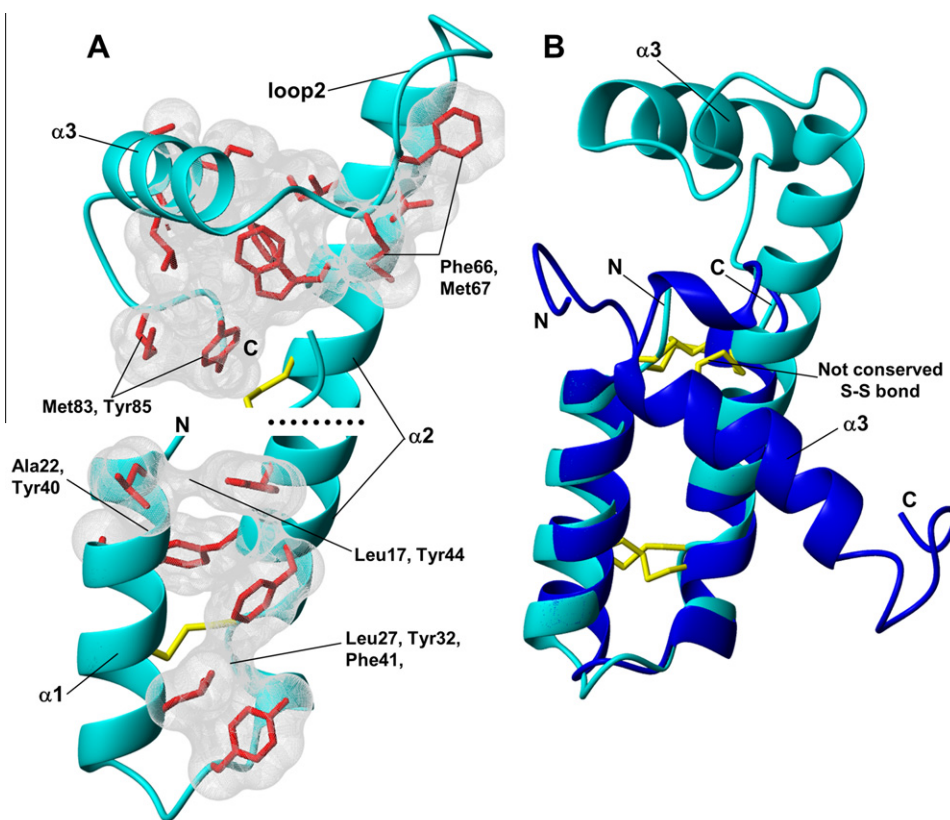

Fig.7. Hydrophobic interactions in the α-helices of CHCHD7$_{2S-S}$ and comparison between CHCHD7$_{2S-S}$ and p8-MTC1 structures. (A) Ribbon presentation of CHCHD7$_{2S-S}$ showing the hydrophobic residues involved in interhelical contacts displayed with van der Waals contact surfaces. Disulfide bonds are shown in yellow; (B) superimposition of the solution structures of CHCHD7$_{2S-S}$ (cyano) and p8-MTC1 (blue). Disulfide bonds are colored in yellow and the not conserved disulfide bond of p8-MTC1 is indicated. The N-terminus and C-terminus are indicated by N and C, respectively. (For interpretation of the references to color in this figure legend, the reader is referred to the web version of this article.)

Cox17). The extended part of helix α2 not included in the CHCH domain interacts with the C-terminal helix α3 (Fig. 6B). In the CHCH domain the hydrophobic interhelical interactions involving residues Leu17, Ala22, Leu27 in helix α1, Tyr44, Tyr40, Phe41 in helix α2, and Tyr32 in the loop does not define a compact patch (Fig. 7A). This suggests that the disulfide bonds play the main role to maintain the interhelical contacts. On the contrary, extensive hydrophobic interactions involving several residues are present between helix α3 and the part of helix α2 not included in the CHCH domain (Fig. 7A). Two residues, Phe66 and Met67, of the loop connecting helix α2 with helix α3 (loop 2) and Met83 and Tyr85 at the C-terminus are also in contact with the interhelical hydrophobic patch, thus determining a well-defined conformation of the loop and of the C-terminal tail (Fig. 7A). Helix α2 is amphipatic having all the hydrophobic residues on the internal side of the structure, being this a fundamental aspect to firmly stick helix α3 to helix α2. In accordance with the numerous interhelical interactions, ^{15}N backbone relaxation properties show that the protein is essentially a rigid molecule with also the loops connecting the helices not showing a high degree of motions (Fig. S6). The anisotropy of rotational diffusion tensor has been characterized by the program TENSOR 2.0 (Dosset et al., 2000) using the relaxation rate R_2/R_1 ratios at 500 MHz and the statistical significance of the description was then investigated. Residues recognized from their relaxation behavior to be rigid were selected for inclusion in the calculation of the anisotropic diffusion tensor following exclusion criteria described in (Tjandra et al., 1995;Cordier et al., 1998), retaining 54 residues. The protein exhibits significant anisotropic reorientation with a diffusion tensor with principal axes values of 2.181×10^7, 1.361×10^7 and 1.485×10^7 s^{-1}. A statistically better fit for the relaxation data was obtained by using the axially symmetric model over the isotropic model. The prolate approximation reproduces the measured relaxation rate ratio better than the oblate approximation ($\chi^2_{pro} = 31.1$ compared to $\chi^2_{obl} = 48.5$). The anisotropic tensorial description is again statistically significant ($\chi^2_{exp} = 30.7$, $\chi^2_{0.05} = 61.7$) but no statistically significant improvement in the fully anisotropic model over axially symmetric diffusion was observed (FTest$_{Exp}$ = 0.50 compared to FTest$_{0.2}$ = 2.82). The relaxation data were analyzed by using both the isotropic and axially symmetric models for the rotational diffusion tensor and, in going from the isotropic to the axially symmetric case, a better fit of the relaxation data was obtained with the axially symmetric model.

In the only other structurally characterized CHCH domain containing a third α-helix, the human p8-MTCP1 (PDB-ID: 2HP8, sequence identity with CHCHD7$_{2S-S}$ 15%) (Barthe et al., 1997), the helices forming the CHCH domain are oriented similarly to those in CHCHD7$_{2S-S}$ (Fig. 7B) preserving indeed the same hydrophobic, interhelical interactions. On the contrary, helix α3 in p8-MTCP1 is oriented differently to that in CHCHD7$_{2S-S}$ (Fig. 7B). This different orientation in p8-MTCP1 with respect to CHCHD7$_{2S-S}$ is determined by: (i) the presence of a further disulfide bond (in addition to those of the CHCH motif) which links the first turn of helix α3 to the last turn of helix α2, and which is absent in CHCHD7$_{2S-S}$ (Fig. 7B); (ii) by the presence of few hydrophobic interactions between helix α3 and the CHCH domain, merely localized at the beginning of helix α3 of p8-MTCP1, at variance with what described before for CHCHD7$_{2S-S}$. Both these features determine the different structural and dynamical properties of helix α3 in p8-MTCP1 with respect to what found for CHCHD7$_{2S-S}$. Indeed, at variance with CHCHD7$_{2S-S}$, helix α3 of p8-MTCP1 shows a progressive increase in both structural disorder and dynamic fluctuations (Barthe et al., 1999, 1997). This comparative analysis confirm that, in CHCHD7$_{2S-S}$, the hydrophobic interactions involving helix α3, helix α2, loop 2 and the C-terminus are crucial to define the orientation of helix α3, and that the reciprocal orientation of the two helical

segments in the CHCH domain is essentially determined by the presence of two disulfide bonds.

4. Discussion

In the CX$_9$C proteins, the structural organization is mainly determined by two different kinds of interhelical interactions: disulfide bonds and hydrophobic contacts. Two typical members of the CX$_9$C protein family whose structures are available are Cox17 (Banci et al., 2008b;Abajian et al., 2004;Arnesano et al., 2005) and Mia40 (Banci et al., 2009;Kawano et al., 2009). The first has an unstructured N-terminal 20-residue-long region followed by the CHCH domain. The second has a CHCH domain interacting with a rigid, N-terminal 20-residue-long region which contains the CPC redox active site, and is surrounded by long unstructured N-terminal (residues 1–41) and C-terminal (residues 107–142) tails. At variance with Cox17, Mia40 has a high degree of hydrophobicity, specifically on one side of the CHCH domain and this hydrophobic region has been found to be essential in the recognition process between Mia40 and the substrates once imported in the IMS through a general entry gate, the outer membrane TOM complex (Chacinska et al., 2009). The degree of hydrophobicity in two helices of each CHCH domain in CHCHD5$_{4S-S}$ is similar to what is found in Mia40, but, overall, more distributed on both sides of the CHCH domains. On the contrary, CHCHD7$_{2S-S}$ is analogous to Cox17, not showing a high level of hydrophobicity in the CHCH domain. However, CHCHD7$_{2S-S}$ has a high degree of hydrophobicity in the extended part of helix α2 and in helix α3, which are both absent in Cox17.

ITS has been found to be responsible for the mitochondrial trapping of this family of CX$_9$C substrates as it is essential for Mia40 protein recognition (Milenkovic et al., 2009;Sideris et al., 2009). Both CHCHD5 and CHCHD7 have putative ITSs and can be thus predicted to be imported in the IMS following a mechanism similar to what already shown for Cox17 (Banci et al., 2009, 2010). Moreover, both proteins have additional hydrophobic regions which can become completely solvent exposed upon disulfide bonds reduction. These data suggest a model where the hydrophobic interactions between Mia40 and the ITSs of CHCHD5/CHCHD7 occur while the other hydrophobic regions of the two Mia40-substrates are not accessible as they are still inside the TOM pore. In such a way, a potential aggregation of CHCHD5 and CHCHD7 can be prevented. This strategy is typically used by molecular chaperones which interact with the nascent proteins preventing self aggregation (Hartl et al., 2011). Following this model, the same process might not be required for Cox17 which indeed, showing a lower degree of hydrophobicity, can interact with Mia40 even when it is completely released from the TOM pore. In the cytosol the possible aggregation phenomena of CHCHD5 and CHCHD7 can be prevented by cytosolic chaperones, particularly heat shock proteins of the Hsp70 and the Hsp90 classes, which have been implicated in the binding of the mitochondrially-imported hydrophobic precursors to transfer them to the TOM complex (Young et al., 2003;Chacinska et al., 2009). A function similar to the molecular chaperone has been proposed for the zinc ion which can play a role in the cytosol during biogenesis of the CHCH proteins, maintaining them in a state appropriate for mitochondrial import through metal binding (Morgan et al., 2009). A further possibility is that IMS-proteins might start to be imported while they are still synthesized (Herrmann and Riemer, 2011). This might be achieved by the attraction of nascent polypeptide chains to the surface of mitochondria so that proteins that are produced by ribosomes are synthesized in direct proximity of the TOM complexes. In agreement with this model, it was shown that mRNAs encoding for mitochondrial proteins are enriched in mitochondrial fractions isolated from

yeast cells (Marc et al., 2002;Eliyahu et al., 2010) and that the mRNA-binding protein Puf3 at the mitochondrial surface (Quenault et al., 2011;Saint-Georges et al., 2008;Garcia-Rodriguez et al., 2007) binds several 5'-UTR regions of mRNA encoding for some IMS proteins including Cox23, the yeast homologue of CHCHD7 (Herrmann and Riemer, 2011).

Acknowledgments

Appendix A. Supplementary data

Supplementary data associated with this article can be found, in the online version, at http://dx.doi.org/10.1016/j.jsb.2012.07.007.

References

Abajian, C., Yatsunyk, L.A., Ramirez, B.E., Rosenzweig, A.C., 2004. Yeast Cox17 solution structure and Copper(I) binding. J. Biol. Chem. 279, 53584–53592.

Arnesano, F., Balatri, E., Banci, L., Bertini, I., Winge, D.R., 2005. Folding studies of Cox17 reveal an important interplay of cysteine oxidation and copper binding. Structure 13, 713–722.

Banci, L., Bertini, I., Calderone, V., Cefaro, C., Ciofi-Baffoni, S., et al., 2012. An electron transfer path through an extended disulfide relay system: the case of the redox protein ALR. J. Am. Chem. Soc. 134, 1442–1445.

Banci, L., Bertini, I., Cefaro, C., Cenacchi, L., Ciofi-Baffoni, S., et al., 2010. Molecular chaperone function of Mia40 triggers consecutive induced folding steps of the substrate in mitochondrial protein import. Proc. Natl. Acad. Sci. USA 107, 20190–20195.

Banci, L., Bertini, I., Cefaro, C., Ciofi-Baffoni, S., Gallo, A., et al., 2009. MIA40 is an oxidoreductase that catalyzes oxidative protein folding in mitochondria. Nat. Struct. Mol. Biol. 16, 198–206.

Banci, L., Bertini, I., Ciofi-Baffoni, S., Gerothanassis, I.P., Leontari, I., et al., 2007a. A structural characterization of human Sco2. Structure 15, 1132–1140.

Banci, L., Bertini, I., Ciofi-Baffoni, S., Hadjiloi, T., Martinelli, M., et al., 2008a. Mitochondrial copper(I) transfer from Cox17 to Sco1 is coupled to electron transfer. Proc. Natl. Acad. Sci. USA 105, 6803–6808.

Banci, L., Bertini, I., Ciofi-Baffoni, S., Janicka, A., Martinelli, M., et al., 2008b. A structural-dynamical characterization of human Cox17. J. Biol. Chem. 283, 7912–7920.

Banci, L., Bertini, I., Ciofi-Baffoni, S., Leontari, I., Martinelli, M., et al., 2007b. Human Sco1 functional studies and pathological implications of the P174L mutant. Proc. Natl. Acad. Sci. USA 104, 15–20.

Barros, M.H., Johnson, A., Tzagoloff, A., 2004. COX23, a Homologue of COX17, Is Required for Cytochrome Oxidase Assembly. J. Biol. Chem. 279, 31943–31947.

Barthe, P., Chiche, L., Declerck, N., Delsuc, M.A., Lefevre, J.F., et al., 1999. Refined solution structure and backbone dynamics of 15N-labeled C12A–p8MTCP1 studied by NMR relaxation. J. Biomol. NMR 15, 271–288.

Barthe, P., Yang, Y.S., Chiche, L., Hoh, F., Strub, M.P., et al., 1997. Solution structure of human p8MTCP1, a cysteine-rich protein encoded by the MTCP1 oncogene, reveals a new alpha-helical assembly motif. J. Mol. Biol. 274, 801–815.

Bernini, A., Venditti, V., Spiga, O., Niccolai, N., 2009. Probing protein surface accessibility with solvent and paramagnetic molecules. Prog. Nucl. Magn. Reson. Spectrosc. 54, 278–289.

Bertini, I., Cowan, J.A., Del Bianco, C., Luchinat, C., Mansy, S.S., 2003. Thermotoga maritima IscU. Structural characterization and dynamics of a new class of metallochaperone. J. Mol. Biol. 331, 907–924.

Bhattacharya, A., Tejero, R., Montelione, G.T., 2007. Evaluating protein structures determined by structural genomics consortia. Proteins 66, 778–795.

Case, D. A., Darden, T. A., Cheatham, T. E., Simmerling, C. L., Wang, J., Duke, R. E., Luo, R., Merz, K. M, Wang, B., Pearlman, D. A., Crowley, M., Brozell, S., Tsui, V., Gohlke, H., Mongan, J., Hornak, V., Cui, G., Beroza, P., Schafmeister, C. E., Caldwell, J. W., Ross, W. S., Kollman, P. A. AMBER 10. [8.0]. 2008. San Francisco, CA, University of California.

Cavallaro, G., 2010. Genome-wide analysis of eukaryotic twin CX9C proteins. Mol. Biosyst. 6, 2459–2470.

Chacinska, A., Koehler, C.M., Milenkovic, D., Lithgow, T., Pfanner, N., 2009. Importing mitochondrial proteins: machineries and mechanisms. Cell 138, 628–644.

Chacinska, A., Pfannschmidt, S., Wiedemann, N., Kozjak, V., Sanjuan Szklarz, L.K. et al. 2004. Essential role of Mia40 in import and assembly of mitochondrial intermembrane space proteins. EMBO J. 2004. Oct. 1;23(19.):3735. -46. Epub. 2004. Sep. 9. 23, 3735–3746.

Claros, M.G., 1995. MitoProt, a Macintosh application for studying mitochondrial proteins. Comput. Appl. Biosci. 11, 441–447.

Cordier, F., Caffrey, M., Brutscher, B., Cusanovich, M., Marion, D., et al., 1998. Solution structure, rotational diffusion anisotropy and local backbone dynamics of Rhodobacter capsulatus cytochrome c 2. J. Mol. Biol. 281, 341–361.

Dosset, P., Hus, J.C., Blackledge, M., Marion, D., 2000. Efficient analysis of macromolecular rotational diffusion from heteronuclear relaxation data. J. Biomol. NMR 16, 23–28.

Eghbalnia, H.R., Wang, L., Bahrani, A., Assadi, A., Markley, J.L., 2005. Protein energetic conformational analysis from NMR chemical shifts (PECAN) and its use in determining secondary structural elements. J. Biomol. NMR 32, 71–81.

Eliyahu, E., Pnueli, L., Melamed, D., Scherrer, T., Gerber, A.P., et al., 2010. Tom20 mediates localization of mRNAs to mitochondria in a translation-dependent manner. Mol. Cell Biol. 30, 284–294.

Farrow, N.A., Muhandiram, R., Singer, A.U., Pascal, S.M., Kay, C.M., et al., 1994. Backbone dynamics of a free and phosphopeptide-complexed Src homology 2 domain studied by 15N NMR relaxation. Biochemistry 33, 5984–6003.

Gabriel, K., Milenkovic, D., Chacinska, A., Muller, J., Guiard, B., et al., 2007. Novel mitochondrial intermembrane space proteins as substrates of the MIA import pathway. J. Mol. Biol. 365, 612–620.

Garcia de la Torre, J.G., Huertas, M.L., Carrasco, B., 2000. HYDRONMR: prediction of NMR relaxation of globular proteins from atomic-level structures and hydrodynamic calculations. J. Magn. Reson. 147, 138–146.

Garcia, d.l.T., Huertas, M.L., Carrasco, B., 2000. HYDRONMR: prediction of NMR relaxation of globular proteins from atomic-level structures and hydrodynamic calculations. J. Magn. Reson. 147, 138–146.

Garcia-Rodriguez, L.J., Gay, A.C., Pon, L.A., 2007. Puf3p, a Pumilio family RNA binding protein, localizes to mitochondria and regulates mitochondrial biogenesis and motility in budding yeast. J. Cell Biol. 176, 197–207.

Grumbt, B., Stroobant, V., Terziyska, N., Israel, L., Hell, K., 2007. Functional characterization of Mia40p, the central component of the disulfide relay system of the mitochondrial intermembrane space. J. Biol. Chem. 282, 37461–37470.

Grzesiek, S., Bax, A., 1993. The importance of not saturating H2O in protein NMR. Application to sensitivity enhancement and NOE measurements. J. Am. Chem. Soc. 115, 12593–12594.

Güntert, P., 2004. Automated NMR structure calculation with CYANA. Methods Mol. Biol. 278, 353–378.

Hartl, F.U., Bracher, A., Hayer-Hartl, M., 2011. Molecular chaperones in protein folding and proteostasis. Nature 475, 324–332.

Hell, K., 2008. The Erv1-Mia40 disulfide relay system in the intermembrane space of mitochondria. Biochim. Biophys. Acta 1783, 601–609.

Herrmann, J.M., Riemer, J., 2011. The mitochondrial disulfide relay: redox-regulated protein import into the intermembrane space. J. Biol. Chem. 287, 4426–4433.

Herrmann, T., Güntert, P., Wüthrich, K., 2002a. Protein NMR structure determination with automated NOE assignment using the new software CANDID and the torsion angle dynamics algorithm DYANA. J. Mol. Biol. 319, 209–227.

Herrmann, T., Güntert, P., Wüthrich, K., 2002b. Protein NMR structure determination with automated NOE-identification in the NOESY spectra using the new software ATNOS. J. Biomol. NMR 24, 171–189.

Horng, Y.C., Cobine, P.A., Maxfield, A.B., Carr, H.S., Winge, D.R., 2004. Specific copper transfer from the Cox17 metallochaperone to both Sco1 and Cox11 in the assembly of yeast cytochrome c oxidase. J. Biol. Chem. 279, 35334–35340.

Kawano, S., Yamano, K., Naoe, M., Momose, T., Terao, K., et al., 2009. Structural basis of yeast Tim40/Mia40 as an oxidative translocator in the mitochondrial intermembrane space. Proc. Natl. Acad. Sci. USA 106, 14403–14407.

Kay, L.E., Torchia, D.A., Bax, A., 1989. Backbone dynamics of proteins as studied by 15N inverse detected heteronuclear NMR spectroscopy: application to staphylococcal nuclease. Biochemistry 28, 8972–8979.

Keller, R., 2004. The Computer Aided Resonance Assignment Tutorial. CANTINA Verlag, Goldau.

Larkin, M.A., Blackshields, G., Brown, N.P., Chenna, R., McGettigan, P.A., et al., 2007. ClustalW and ClustalX version 2.0. Bioinformatics 23, 2947–2948.

Lee, L.K., Rance, M., Chazin, W.J., Palmer, A.G., III. 1997. Rotational diffusion anisotropy of proteins from simultaneous analysis of 15N and 13C alpha nuclear spin relaxation. J. Biomol. NMR 9, 287–298.

Lionaki, E., Aivaliotis, M., Pozidis, C., Tokatlidis, K., 2010. The N-terminal shuttle domain of Erv1 determines the affinity for Mia40 and mediates electron transfer to the catalytic Erv1 core in yeast mitochondria. Antioxid. Redox. Signal. 13, 1327–1339.

Longen, S., Bien, M., Bihlmaier, K., Kloeppel, C., Kauff, F., et al., 2009. Systematic analysis of the twin cx(9)c protein family. J. Mol. Biol. 393, 356–368.

Madani, A., Soulier, J., Schmid, M., Plichtova, R., Lerme, F., et al., 1995. The 8 kD product of the putative oncogene MTCP-1 is a mitochondrial protein. Oncogene 10, 2259–2262.

Marc, P., Margeot, A., Devaux, F., Blugeon, C., Corral-Debrinski, M., et al., 2002. Genome-wide analysis of mRNAs targeted to yeast mitochondria. EMBO Rep. 3, 159–164.

Mesecke, N., Terziyska, N., Kozany, C., Baumann, F., Neupert, W., et al., 2005. A disulfide relay system in the intermembrane space of mitochondria that mediates protein import. Cell 121, 1059–1069.

Milenkovic, D., Ramming, T., Muller, J.M., Wenz, L.S., Gebert, N., et al., 2009. Identification of the signal directing Tim9 and Tim10 into the intermembrane space of mitochondria. Mol. Biol. Cell 20, 2530–2539.

Molinari, H., Esposito, G., Ragona, L., Pegna, M., Niccolai, N., et al., 1997. Probing protein structure by solvent perturbation of NMR spectra: the surface accessibility of bovine pancreatic trypsin inhibitor. Biophys. J. 73, 382–396.

Morgan, B., Ang, S.K., Yan, G., Lu, H., 2009. Zinc can play chaperone-like and inhibitor roles during import of mitochondrial small Tim proteins. J. Biol. Chem. 284, 6818–6825.

Neupert, W., Herrmann, J.M., 2007. Translocation of proteins into mitochondria. Annu. Rev. Biochem. 76, 723–749.

Quenault, T., Lithgow, T., Traven, A., 2011. PUF proteins: repression, activation and mRNA localization. Trends Cell Biol. 21, 104–112.

Roy, A., Kucukural, A., Zhang, Y., 2010. I-TASSER: a unified platform for automated protein structure and function prediction. Nat. Protoc. 5, 725–738.

Saint-Georges, Y., Garcia, M., Delaveau, T., Jourdren, L., Le Crom, S., et al., 2008. Yeast mitochondrial biogenesis: a role for the PUF RNA-binding protein Puf3p in mRNA localization. PLoS One 3, e2293.

Sharma, D., Rajarathnam, K., 2000. 13C NMR chemical shifts can predict disulfide bond formation. J. Biomol. NMR 18, 165–171.

Shen, Y., Delaglio, F., Cornilescu, G., Bax, A., 2009. TALOS plus: a hybrid method for predicting protein backbone torsion angles from NMR chemical shifts. J. Biomol. NMR 44, 213–223.

Sideris, D.P., Petrakis, N., Katrakili, N., Mikropoulou, D., Gallo, A., et al., 2009. A novel intermembrane space-targeting signal docks cysteines onto Mia40 during mitochondrial oxidative folding. J. Cell Biol. 187, 1007–1022.

Soulier, J., Madani, A., Cacheux, V., Rosenzwajg, M., Sigaux, F., et al., 1994. The MTCP-1/c6.1B gene encodes for a cytoplasmic 8 kD protein overexpressed in T cell leukemia bearing a t(X;14) translocation. Oncogene 9, 3565–3570.

Terziyska, N., Grumbt, B., Bien, M., Neupert, W., Herrmann, J.M., et al., 2007. The sulfhydryl oxidase Erv1 is a substrate of the Mia40-dependent protein translocation pathway. FEBS Lett. 581, 1098–1102.

Terziyska, N., Grumbt, B., Kozany, C., Hell, K., 2009. Structural and functional roles of the conserved cysteine residues of the redox-regulated import receptor Mia40 in the intermembrane space of mitochondria. J Biol. Chem. 284, 1353–1363.

Tjandra, N., Feller, S.E., Pastor, R.W., Bax, A., 1995. Rotational diffusion anisotropy of human ubiquitin from 15N NMR relaxation. J. Am. Chem. Soc. 117, 12562–12566.

Tsan, P., Hus, J.C., Caffrey, M., Marion, D., Blackledge, M., 2000. Rotational diffusion anisotropy and local backbone dynamics of carbon monoxide bound Rhodobacter capsulatus cytochrome c'. J. Am. Chem. Soc. 122, 5603–5612.

Wishart, D.S., Sykes, B.D., Richards, F.M., 1992. The chemical shift index: a fast and simple method for the assignment of protein secondary structure through NMR spectroscopy. Biochemistry 31, 1647–1651.

Young, J.C., Hoogenraad, N.J., Hartl, F.U., 2003. Molecular chaperones Hsp90 and Hsp70 deliver preproteins to the mitochondrial import receptor Tom70. Cell 112, 41–50.

Zhang, Y., 2008. I-TASSER server for protein 3D structure prediction. BMC Bioinf. 9, 40.

Zhang, Y., Skolnick, J., 2004. Scoring function for automated assessment of protein structure template quality. Proteins 57, 702–710.